UC Berkeley
UC Berkeley Previously Published Works

Title
Influence of the Substrate on the Creep of SN Solder Joints

Permalink
https://escholarship.org/uc/item/4578497j

Journal
Metallurgical and Materials Transactions A, 41(7)

ISSN
1543-1940

Authors
Lee, K.-O.
Morris, J.W.
Hua, F.

Publication Date
2010-07-01

DOI
10.1007/s11661-010-0214-6

Peer reviewed

eScholarship.org Powered by the California Digital Library
University of California

Influence of the Substrate on the Creep of SN Solder Joints

K.-O. LEE, J.W. MORRIS, Jr., and F. HUA

The creep rate of Sn solder joints is noticeably affected by joint metallization. Cu|Sn|Cu joints have significantly higher creep rates than Ni|Sn|Cu joints, which, in turn, have higher creep rates than Ni|Sn|Ni joints. Replacing Ni by Cu on both substrates increases the creep rate at 333 K (60 °C) by roughly an order of magnitude. The increased creep rate appears with no apparent change in the dominant creep mechanism; the change in the constitutive equation for creep (the Dorn equation) is in the pre-exponential factor. The decreased creep rate on substituting Ni is accompanied by an increase in the hardness of the polygranular solder but a decrease in the nanohardness of the grain interiors. The source of the strong influence of the Ni substrate appears to be the introduction of an array of Ni_3Sn_4 intermetallic precipitates along the grain boundaries. These precipitates inhibit grain boundary sliding, boundary reconfiguration, and grain growth during creep. The intermediate creep rate of the asymmetric Ni|Sn|Cu joint has two causes: a decrease in grain boundary mobility due to precipitate decoration and a restriction in the free volume of the joint due to rapid intermetallic growth from the substrate on the Ni side. The sources of this anomalous intermetallic growth are discussed.

DOI: 10.1007/s11661-010-0214-6
© The Author(s) 2010. This article is published with open access at Springerlink.com

I. INTRODUCTION

CONCERN over the toxicity of lead has led to the introduction of Pb-free solders in microelectronic devices. The most widely used are high-Sn alloys with small additions of Ag or Cu. The properties of the Sn matrix ordinarily dominate the mechanical behavior of these high-Sn alloys. Since Sn has a complex crystal structure and anisotropic mechanical properties that have not been thoroughly explored, the reliability of Sn-rich solder joints is of some concern. The creep behavior of high-Sn joints is particularly important, since the low melting temperatures of solder alloys have the consequence that creep is the dominant deformation mechanism, even at room temperature.[1] Given the technological need, there is an increasing body of published research on the creep of high-Sn alloys.[2–7] However, most of this work describes the creep of the alloys in bulk form. Solders in microelectronic joints may have microstructures and, hence, mechanical properties that differ significantly from those found in bulk samples.[8] The manufacture of fine-pitch solder joints ordinarily includes processes such as rapid solidification and reactions between the solder and the substrate that may create compositions and textures that are very different from those encountered in bulk samples.[9,10] Solder joints also contain interfacial intermetallic layers that may influence creep behavior.

The present work was undertaken to study the influence of the substrate metallization on the creep of Sn-rich solder joints. To simplify the interpretation of the results, we used pure Sn as the solder rather than conventional ''Pb-free'' solders, which include small additions of Ag and Cu. The substrate pairs were Cu-Cu, Cu-Ni, and Ni-Ni, all of which are commonly found in microelectronic devices.

II. EXPERIMENTAL PROCEDURE

The geometry of the creep specimens used in this study is shown in Figure 1. Flat OFHC Cu plates were overlapped into a single-lap shear configuration and joined by a 3 × 3 pattern of 9 solder joints. The solder joints were located by making small, raised lands on the surfaces of the Cu plates. These were either used as-made for Cu substrates or plated with ~4-μm electroless Ni coated with 0.13-μm Au to form the Ni substrates.

The solder was made in the form of pure Sn foils that were melted, cast in Cu blocks and homogenized for 48 hours at 443 K (170 °C) before being rolled to 180 μm thickness. Pieces were cut from the Sn foils, inserted between the lands on the Cu blocks, and reflowed to form the solder joints. The reflow was done in two steps: 418 K (145 °C) for 5 minutes followed by 518 K (245 °C) for 8 minutes in a programmable oven under nitrogen gas.

The creep tests were done in a dead-load creep machine with temperature controlled by an oil bath, held at 333 K (60 °C) for the tests reported here. Details of the creep test procedure have been reported elsewhere.[8] The shear stress was measured as shear load divided by the solder-substrate contact area (the total

K.-O. LEE, formerly Ph.D. Candidate, with the Department of Materials Science and Engineering, University of California, is Packaging Engineer, Substrate Pathfinding, Assembly and Test Technology Development, Intel Corporation, Chandler, AZ 85226. Contact e-mail: kyu-oh.lee@intel.com J.W. MORRIS, Jr., Professor of Metallurgy, is with the Department of Materials Science and Engineering, University of California, Berkeley, CA 94720. F. HUA, Senior Packaging Engineer, is with Components Research, Intel Corporation, Sunnyvale, CA 95054.

Manuscript submitted June 24, 2007.
Article published online April 21, 2010

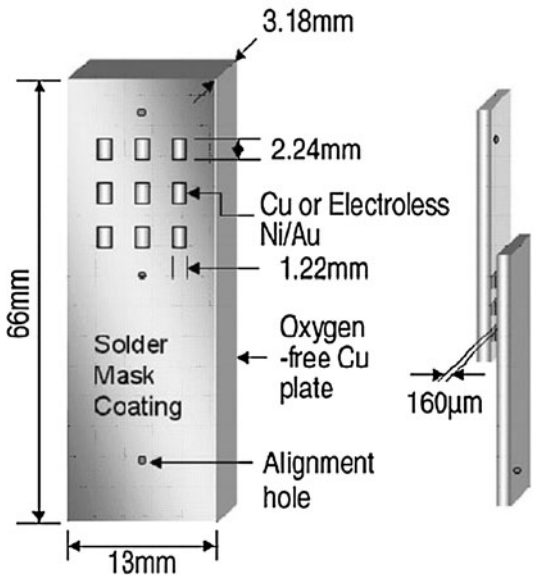

Fig. 1—Schematic diagram showing the specimen geometry.

area of the wetted pads). The shear strain (simple shear) was measured as the relative displacement of the sample plates divided by the solder joint thickness. The reported creep rates are steady-state creep rates.

Micro- and nanohardnesses were used to characterize the basic mechanical properties of the solders. Since the crystallographic anisotropy of Sn affects the nanohardness values, nanoindentations were done on the interiors of grains with known crystallographic orientation. To achieve this, samples were prepared, as illustrated in Figure 2. One side of the solder joint was polished, and areas on the surface were etched with a focused ion beam (FIB), using glancing incidence to minimize ion beam damage and leave a flat surface whose orientation could be revealed by electron backscattered diffraction (EBSD). The prepared surface was then indented at 16 to 25 separate positions, depending upon the grain size, using a Hysitron Triboindenter (Minneapolis, MN) operated under load control with a peak load of 25 to 50 nN. The grain orientations were then mapped by EBSD, using the TSL Orientation Imaging Microscopy system,[11] so that the hardness readings could be associated with specific crystallographic orientations.

To study changes in the microstructure during creep, EBSD was also used to measure the distribution of grain boundary misorientations before and after creep at the same location and at the same solder joint. These measurements were combined with optical microscopy, scanning electron microscopy (SEM), and transmission electron microscopy (TEM) studies to clarify the influence of microstructure and microstructural changes on creep behavior.

III. RESULTS AND DISCUSSION

The creep tests reported here were done under load (stress) control with the strain measured as a function of time to generate creep curves. The steady-state strain rates were measured from the linear portions of the creep curves and plotted against the stress in logarithmic plots such as that shown in Figure 3. As is common in high-temperature creep, the data divide into segments that are individually well fit by constitutive equations of the Dorn form:[12,13]

$$\dot{\gamma} = A\frac{G\mathbf{b}}{\mathrm{k}T}\left[\frac{\tau}{G}\right]^{n}\exp[-Q/\mathrm{k}T] \qquad [1]$$

where $\dot{\gamma}$ is the shear strain rate, τ is the shear stress, G is the shear modulus, $\mathbf{b}$ is the Burgers vector, Q is the activation energy, $\mathrm{k}T$ is the Boltzmann temperature, and A is a pre-exponential factor. The different segments of the creep curve for a given material and temperature ordinarily correspond to different dominant creep mechanisms, which generate different values of the stress exponent, n, activation energy, Q, or both.

Figure 3 shows the measured steady-state creep rate as a function of stress for pure Sn joints tested at 333 K (60 °C) for the three substrate combinations: Cu-Cu, Cu-Ni, and Ni-Ni. The results are typical of a number of independent tests. The three curves are almost identical in shape. Each divides into two segments with different stress exponents. While the data set is insufficient to determine precise values of the stress exponents, $n \sim 7$ in the high stress region and is near 3 at low stress, with the change in mechanism at $\tau \sim 5$ MPa. These results are in general agreement with those of Chawla *et al.*, though there are small differences in the stress exponents.[14] Possible creep mechanisms have been discussed by others (for example, Reference 15), but were not specifically investigated in this work.

To within the accuracy of the data taken here, the stress exponents were not affected by the substrate metallization. However, the creep rate at given stress changes significantly. The Cu-Cu joint creeps at a rate that is roughly an order of magnitude faster than the Ni-Ni joint at a given stress level, with the Cu-Ni rates in between. An order of magnitude difference in creep rate has potential technological consequences, so this difference needs to be understood.

Since the properties of a given material are determined by its microstructure, we investigated several microstructural differences that might play a role, including the nature of the interfacial intermetallic, the crystallographic texture of the solidified Sn, the grain size, and the precipitate distribution, particularly including intergranular precipitates.

A. *Interfacial Intermetallics*

The solder is bonded to the metallized lands on each side by intermetallic layers. The substrate influences both the nature and morphology of these intermetallics. As we have discussed in a previous report,[16] the dominant intermetallic in both the Cu-Cu and Cu-Ni couples is Cu_6Sn_5, while in the Ni-Ni couple, it is Ni_3Sn_4. Since the intermetallic layers are neither deformed nor fractured during the creep tests done here, the chemical nature of the intermetallic layer should not affect the creep rate. On the other hand, the

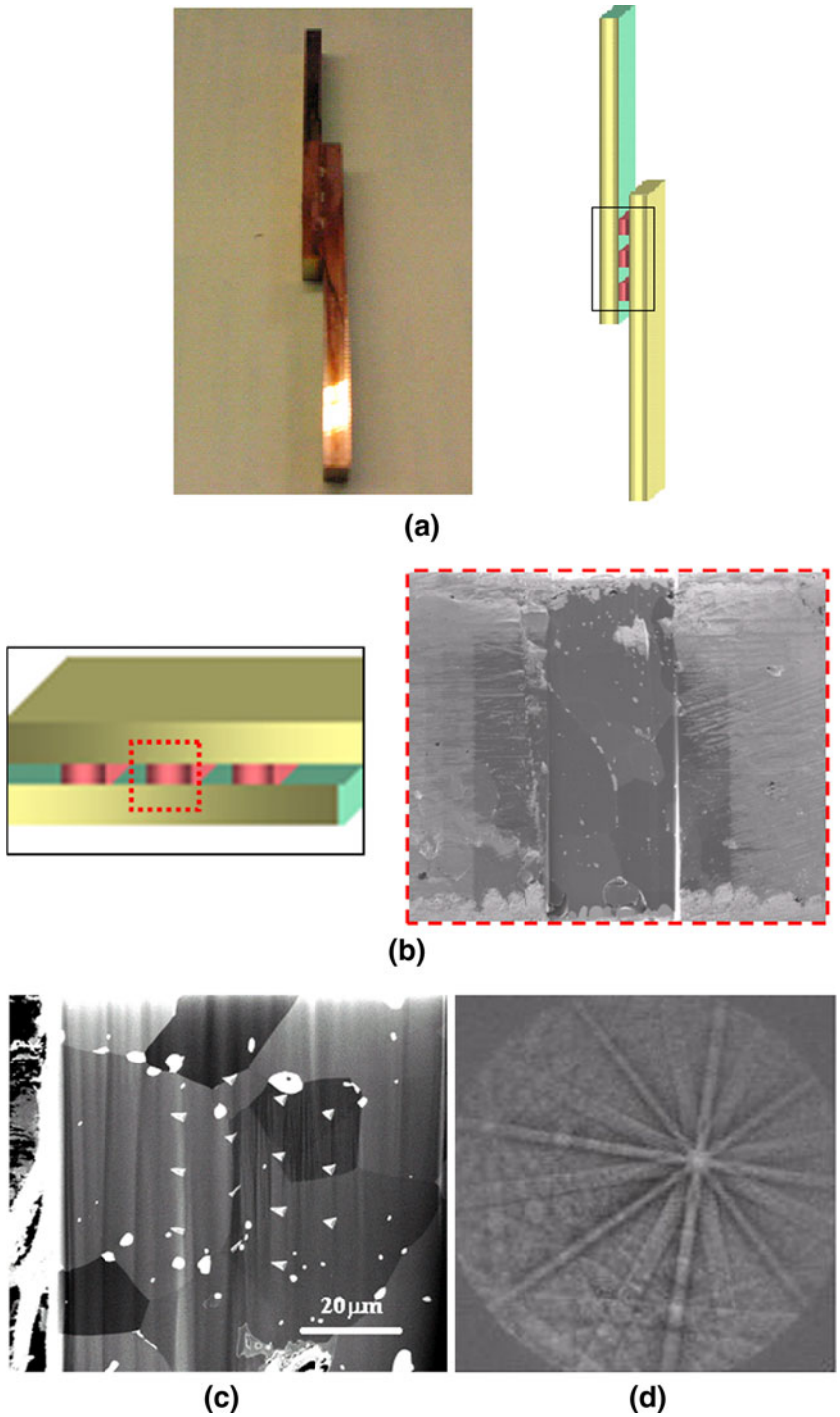

Fig. 2—Sample preparation for the nanoindentation and EBSD analysis: (*a*) mechanical polishing, (*b*) etching with FIB, (*c*) nanoindentation, and (*d*) EBSD on the indentation area.

morphology of the intermetallic layer does play a role, particularly in the case of the asymmetric Cu-Ni couple.

Figure 4 shows the intermetallic layer morphology for the Cu-Cu and Cu-Ni substrate systems, as revealed by etching before and after deformation in creep. The Ni-Cu joint has an anomalous, asymmetric layer morphology: the interfacial intermetallic has thickened dramatically on the Ni side, generating nominally Cu_6Sn_5 whiskers that extend well into the body of the solder joint.[16]

The marker tests illustrated in Figure 4(a) show that these projections serve to pin the solder against creep; almost all of the deformation occurs in the bulk solder beyond the reach of the projecting whiskers. It follows that the effective strain rate in the Ni-Cu couple, that is, the strain rate in that part of the cross section that is

actually being strained, is significantly higher than given in Figure 3. The data were corrected for this effect and the results plotted in Figure 5. As can be seen from Figure 5, the intermetallic morphology has a significant effect on the creep rate of the Ni-Cu sample. This effect accounts for roughly half the difference between the nominal creep rates of the Ni-Cu and Cu-Cu samples.

However, the intermetallic morphology provides only a partial explanation for the substrate effects observed here. It does not explain the substantial difference between the Cu-Cu and Ni-Ni samples and explains only part of the discrepancy between the Ni-Cu and Cu-Cu samples.

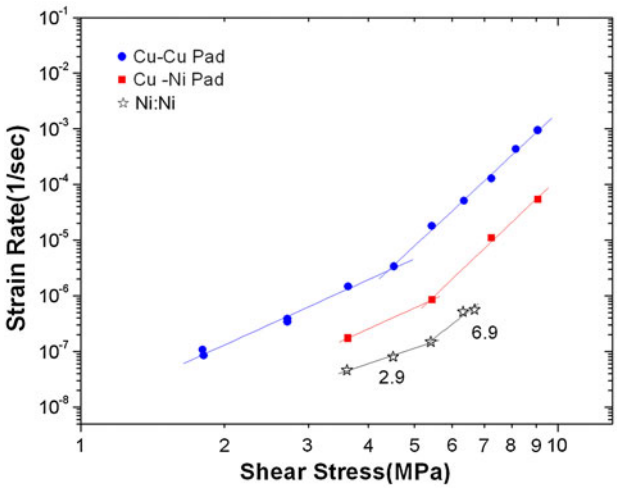

Fig. 3—Creep properties of pure Sn solder joints at 333 K (60 °C) with three different substrate combinations: Cu-Cu, Cu-Ni, and Ni-Ni.

B. *Texture*

β-Sn has a tetragonal crystal structure that causes a significant anisotropy in its mechanical properties. For example, its elastic modulus has a strong directional dependence. It is possible, therefore, that its creep behavior is anisotropic as well. If this is true, the overall creep rates of Sn-rich solder joints may depend on their crystallographic texture, which may be influenced by the substrate metal. In fact, pronounced textures have been observed in Pb-free solder joints.[17] We therefore measured the crystallographic textures of a number of solder joints made with each of our substrate combinations.

The results of our texture measurements are presented in Figure 6, which shows [001] pole figures for four different samples of each joint couple after creep. In these pole figures, the *c*-axis, [001], of the β-Sn structure was set perpendicular to the substrate plane. While each sample has a pronounced texture, the texture varies and shows about as much variation between examples of the same couple as it does between couples. These and other results suggest that the dominant source of texture may simply be the direction of cooling; the [100] or [110] direction in the joints tends to tilt toward the fan used to cool the joints.

To explore the texture effect further, we performed microhardness tests on the solder joints, using an indenter large enough to sample several grains and

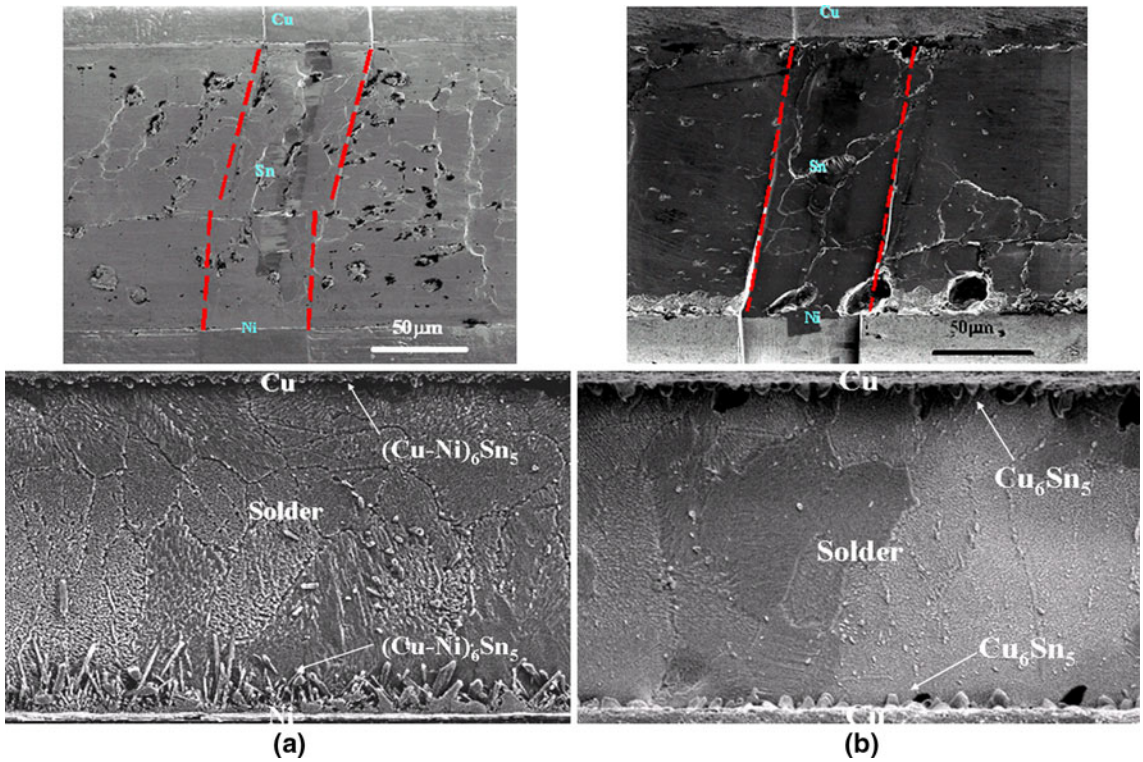

Fig. 4—Interfacial intermetallic effect on the overall creep deformation behavior of the solder joints with (*a*) Ni-Cu and (*b*) Cu-Cu metallization.

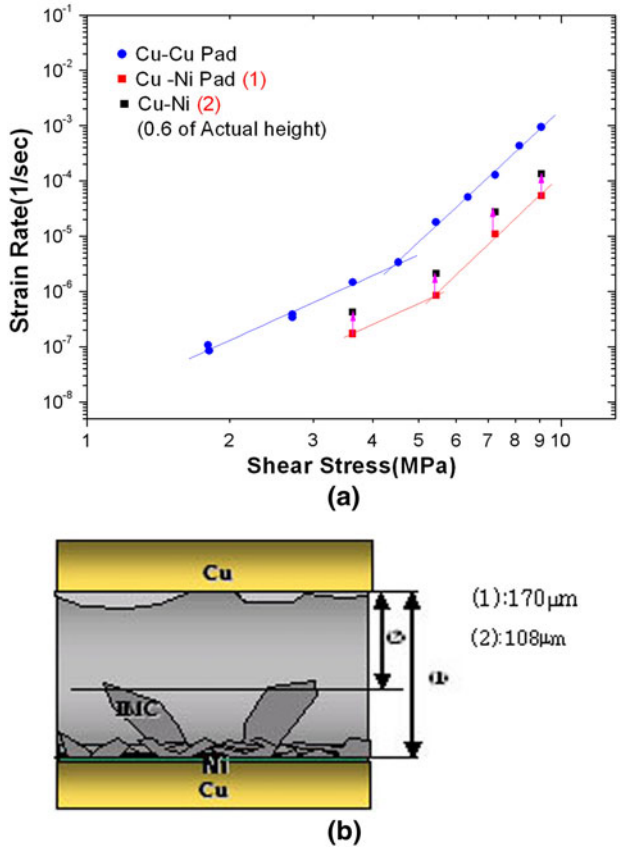

Fig. 5—Creep rates corrected for the anomalous thickness of the interfacial intermetallic in the Cu-Ni couple.

capture the local texture. The results are shown in Figure 7. They show an interesting and direct correspondence to the creep data; hardness increases in the sequence Cu-Cu, Ni-Cu, Ni-Ni, just as the creep resistance does. The differences between the different metallizations are significant, and larger than the scatter in tests on samples with the same metallization. The differences are not related to texture in any obvious way. Samples from a given couple with very different textures have similar hardnesses, while samples with similar texture, but different metallization, have significantly different hardnesses.

Creep tests were also done on samples with distinct textures. While the limited data set is not sufficient to reveal subtle texture effects, there is no obvious influence on the creep rate.

We, therefore, conclude that crystallographic texture is not the dominant variable determining creep resistance. However, the correspondence between microhardness and creep resistance suggests that there is an underlying microstructural difference that influences both.

C. *Grain Size*

When samples of similar chemistry have different hardnesses, the usual hypothesis is that they differ in grain size and obey a hardening relation of the Hall–Petch form. To test this hypothesis, we used SEM

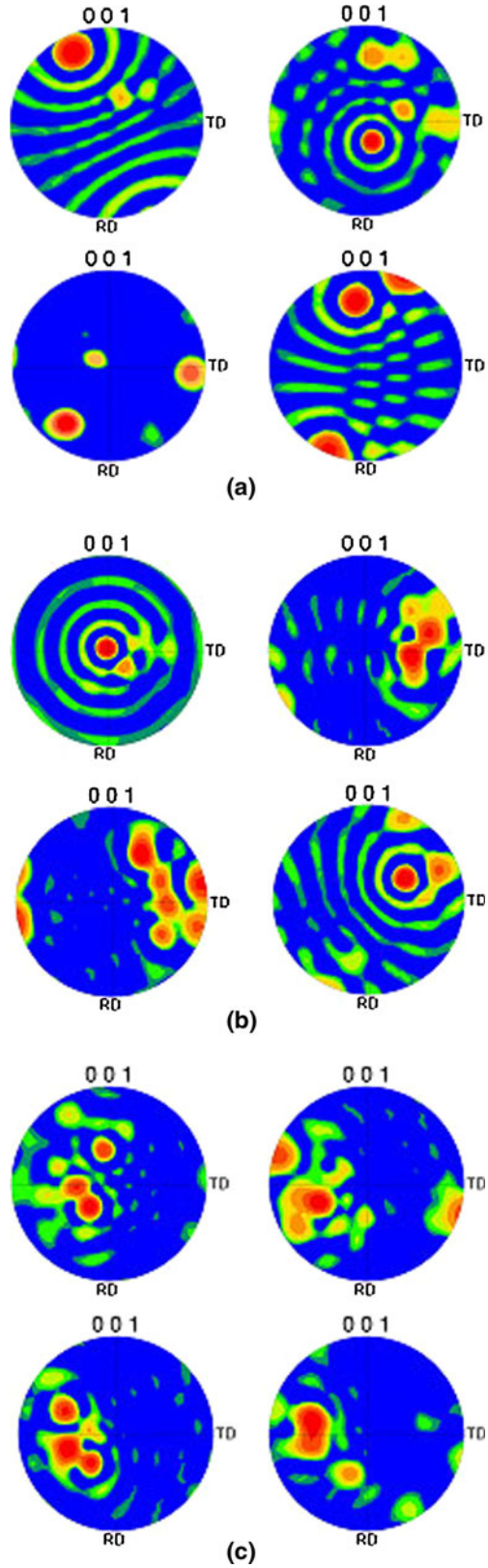

Fig. 6—⟨001⟩ pole figures of four different β-Sn joints after reflow with metallizations: (*a*) Cu:Cu, (*b*) Ni:Cu, and (*c*) Ni:Ni.

images to measure the apparent grain sizes of joints with different substrate metallization. Examples of the results are shown in Figure 8. The Cu-Cu and Ni-Cu couples

had mean grain sizes of about 12 μm, while the Ni-Ni samples had significantly smaller grain size, near 6 μm. These results are consistent with the high hardness of the Ni-Ni samples, but cannot explain the significant difference in hardness between the Cu-Cu and Ni-Cu samples.

The influence of grain size on the creep properties is, in fact, the inverse of what is often observed. The creep rate often increases in fine-grained structures, due to the influence of grain boundary sliding. However, in this case, the fine-grained structures have the lowest creep rates. This result suggests that the grain boundaries are effectively pinned in the fine-grained joint between the Ni-Ni couple and do not undergo significant grain boundary sliding.

D. *Matrix Hardening*

If the grain size cannot explain the hardness (or, at least, cannot explain all of it), we are led to ask if there is a significant difference in the hardness of the bulk material within the grains, particularly given the expectation, documented by Chawla *et al.*,[18] that the size and distribution of intragranular precipitates affect the creep behavior. We, therefore, used nanoindentation tests to measure the inherent hardness of the material in the grain interiors.

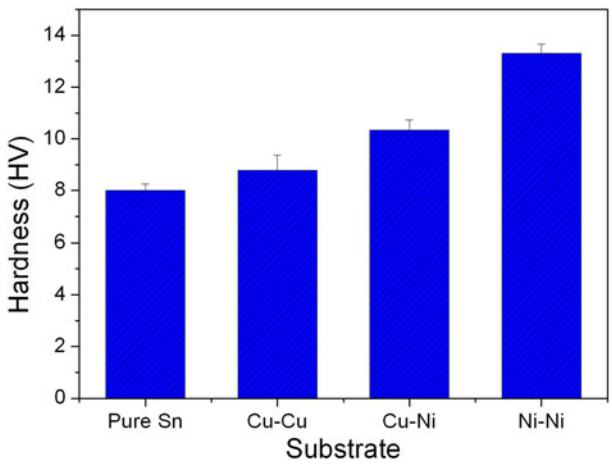

Fig. 7—Change of microhardness with substrate metallization: pure Sn, Cu:Cu, Ni:Cu, and Ni:Ni.

These nanoindentation data had to be gathered with some care. Given the anisotropy of the β-Sn crystal structure, the hardness of a grain interior should depend on the orientation of the grain. To compare the inherent hardness of two samples, we must compare grains that have the same orientation. To accomplish this, we made multiple nanoindentations on polygranular samples of solder joints with each metallization, using EBSD to determine the orientations of the grains that were indented. The procedure is illustrated in Figure 9.

The initially surprising results of the nanoindentation tests are presented in Figure 10. When compared at constant orientation, the Ni-Ni samples were the softest of the three while the Cu-Cu samples were the hardest; the most creep-resistant metallization is that which creates the softest solder. It follows that the hardness of the bulk solder cannot be responsible for the creep resistance we measured.

These observations are, however, consistent with the observed distribution of intragranular precipitates, as observed through scanning electron microscopy. The relatively low-melting β-Sn can be selectively etched with an ion beam, so the intragranular precipitate distributions are revealed in samples lightly etched with FIB. Examples of the precipitate distributions revealed in this way are given in Figure 11. The intragranular precipitate distributions in the Cu-Cu and Ni-Cu joints are dense compared to that in the Ni-Ni joint. This comparative density of precipitates apparently reflects the relatively low solubility and diffusivity of Ni in Sn compared to that of Cu;[19] Cu-Sn intermetallic precipitates are densely distributed through the bulk, while Ni-Sn precipitates are rarely seen.

E. *Grain Boundary Structure and Mobility*

Given that grain boundary sliding can be an effective deformation mechanism in creep, we expect the grain boundary mobility to be an important factor in creep.[17] If a polygranular material is relatively hard while its intragranular material is relatively soft, the reason must lie either in the mobility of the grain boundaries (*i.e.*, in their ability to accomplish strain) or in their resistance to the transmission of strain. We therefore investigated the

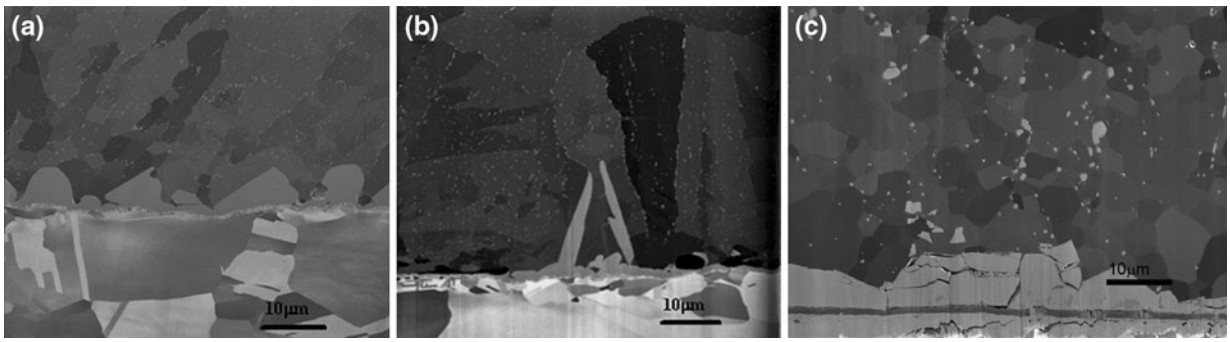

Fig. 8—SEM images showing the overall microstructure of the joints after reflow using the metallizations: (*a*) Cu:Cu, (*b*) Ni:Cu, and (*c*) Ni:Ni.

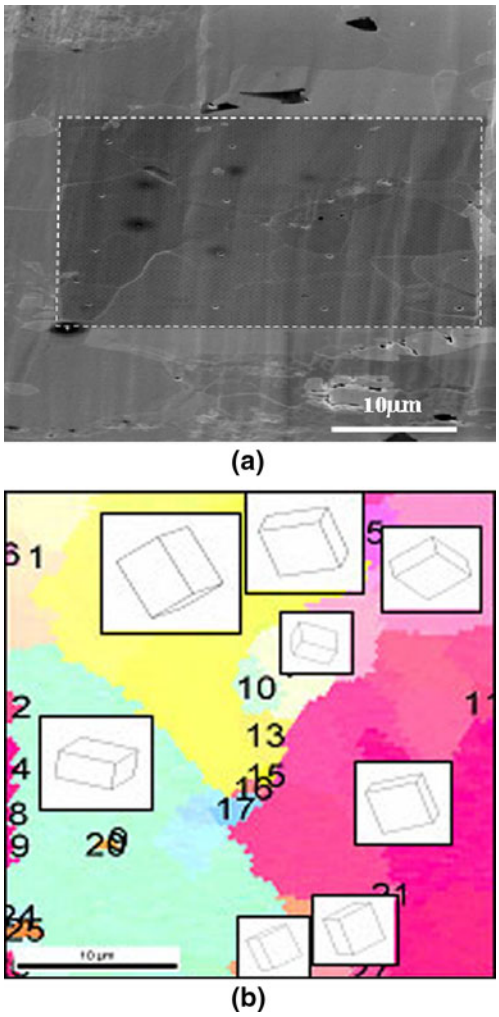

Fig. 9—Typical nanoindentation mark on a pure Sn solder joint and its orientation image mapping with (*a*) SEM and (*b*) EBSD.

structure and mobility of the grain boundaries in joints with the three substrate combinations whose typical creep strain to failure ranges from 0.2 to 0.3, depending upon the test load.

The intergranular precipitate distributions are also revealed by etching, as in Figure 11. While the Ni-Ni joint has a lower density of precipitates within the grains, the density of precipitates on the grain boundaries is the same or larger than in the Cu-Cu and Cu-Ni cases. The precipitates are also smaller in the Ni-Ni case. The fact that the Ni intermetallics are confined to the grain boundaries suggests that it is energetically unfavorable for them to separate from the grain boundaries into the bulk. The fact that these precipitates remain small suggests that they coarsen with difficulty, and hence resist reconfiguration within the boundary. Precipitates that can neither move out of the boundaries nor reconfigure within them, as appears to be the case with the Ni intermetallics, should be much more effective at pinning boundaries than those that are more mobile, as the Cu intermetallics appear to be. Therefore, they should be more effective in producing polygranular hardness and creep resistance, as the Ni intermetallics appear to be.

To explore the issue further, we supplemented the measurement of grain size, reported previously, with EBSD analysis of the nature of the grain boundaries. If the Ni intermetallics are more effective in pinning grain boundaries, then, in addition to increasing strength, they should inhibit the reconfiguration of the grain boundaries during high-temperature exposure, when the grains seek low-energy configurations, and during creep, when the grains will tend to reorient to facilitate plastic deformation. Therefore, we investigated the influence of metallization on grain boundary orientation after reflow and after creep.

Figure 12 presents the distributions of grain boundary misorientations after reflow for the three metallizations used. The data include 20 to 30 grains in each case. The distributions are qualitatively different. The Cu-Cu metallization produces a distribution that is sharply peaked at low angles and near 60 deg, which is the low-energy "twin" orientation,[20] which is evidence for high mobility that allows boundaries to reconfigure into low-energy configurations. The Ni-Ni metallization produces a distribution that is much more random, including many relatively high-energy configurations. This suggests that grain boundaries are effectively pinned. The Cu-Ni metallization yields a distribution that is intermediate between the two, as expected from a mixture of intermetallic precipitate types.

Figure 13 shows the change in the grain boundary distribution after creep under 7.2 MPa load at 333 K (60 °C) in oil. The data were generated by using EBSD to determine the misorientation distributions at the same location before and after the test. The results show a substantial change in the distribution of the Cu-Cu specimen, while there is almost no change in the distribution for the Ni-Ni specimen. The Ni-Cu metallization has an intermediate behavior, more like Cu-Cu than Ni-Ni. These data are, again, consistent with effective grain boundary pinning by the intergranular Ni intermetallics that prevents the reconfiguration of the grain boundaries in response to the strain. Cu intermetallics are less effective in pinning boundaries, so the boundaries reconfigure under strain.

These results show that the grain boundaries in the joint with Ni-Ni metallization are strongly pinned by fine immobile intergranular intermetallic Ni_3Sn_4 precipitates. The restricted mobility of the grain boundaries is the apparent reason for both higher microhardness and greater creep resistance of the Ni-Ni joint. The tendency of these intermetallics to confine themselves to the grain boundaries is an expected consequence of the low bulk diffusivity in Sn.[21] The diffusional flux of Ni is expected to be small except along the boundaries themselves, and low (relative to Cu) even there.

The intermediate behavior of the Ni-Cu couple appears to be due to an intermediate degree of grain boundary decoration that restricts grain boundary mobility, though not as severely as in the Ni-Ni case. While the precipitates have the Cu_6Sn_5 structure, they appear to include some Ni to create $(Cu,Ni)_6Sn_5$. The participation of Ni will decrease the free energy of the precipitate phase, hence promoting its formation. However, that extra precipitation should be concentrated

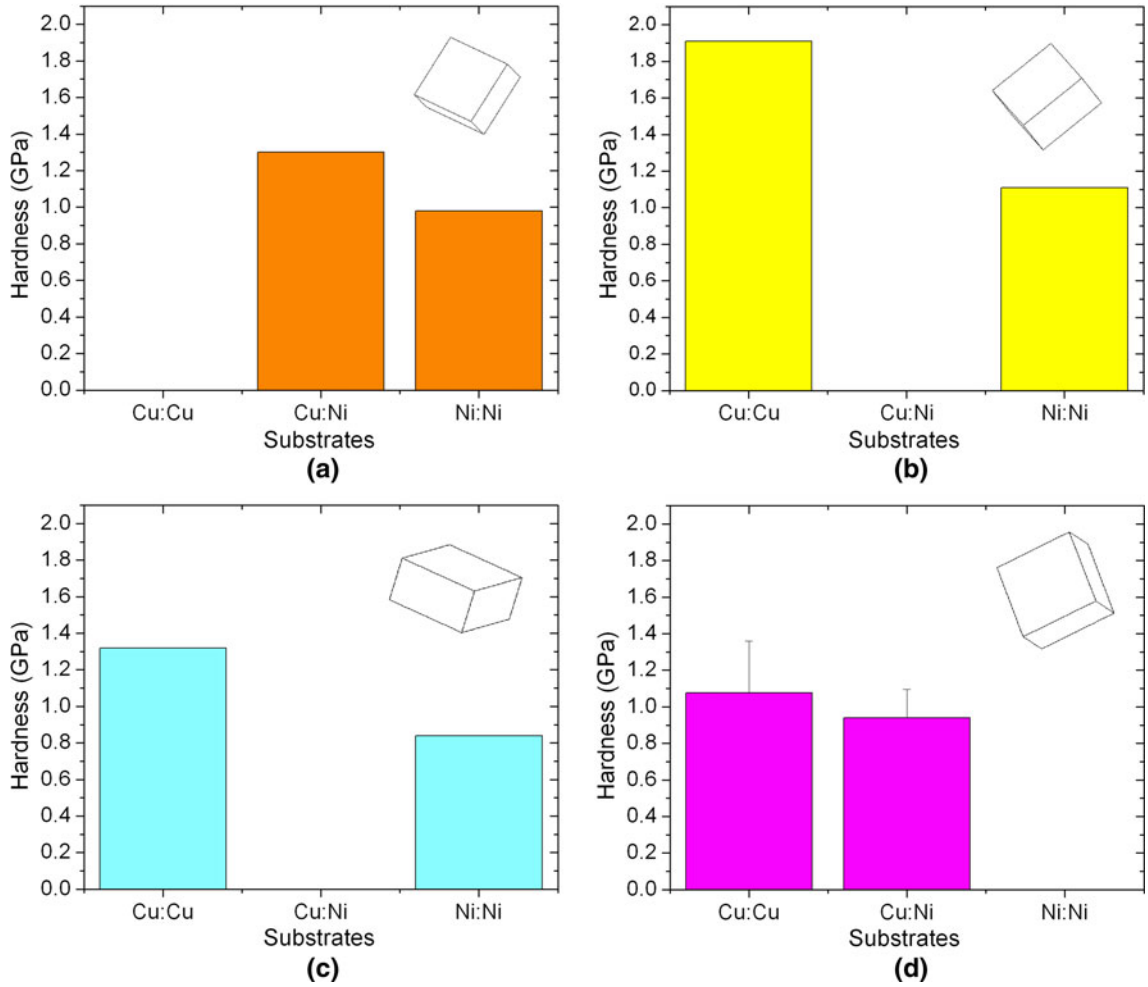

Fig. 10—Comparative nanoindentation hardnesses of different substrate systems, comparing grains with almost identical crystallographic orientations.

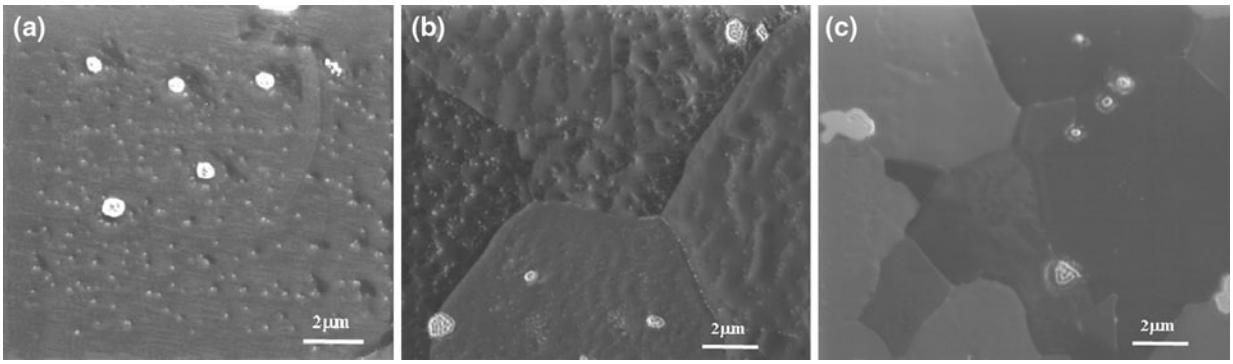

Fig. 11—SEM images showing fine precipitates after ion beam etching of pure Sn solder joints with (*a*) Cu:Cu, (*b*) Ni:Cu, and (*c*) Ni:Ni substrates.

on the grain boundaries where the Ni is kinetically accessible.

The restricted grain boundary mobility appears to be the primary factor that changes the pre-exponential factor, A, in the Dorn Eq. [1] without significantly changing the stress exponent (the activation energy was not measured in this work). This is consistent with the overall creep behavior; while we did not determine activation energies, the creep exponents observed are typical of conventional, bulk creep mechanisms. Creep

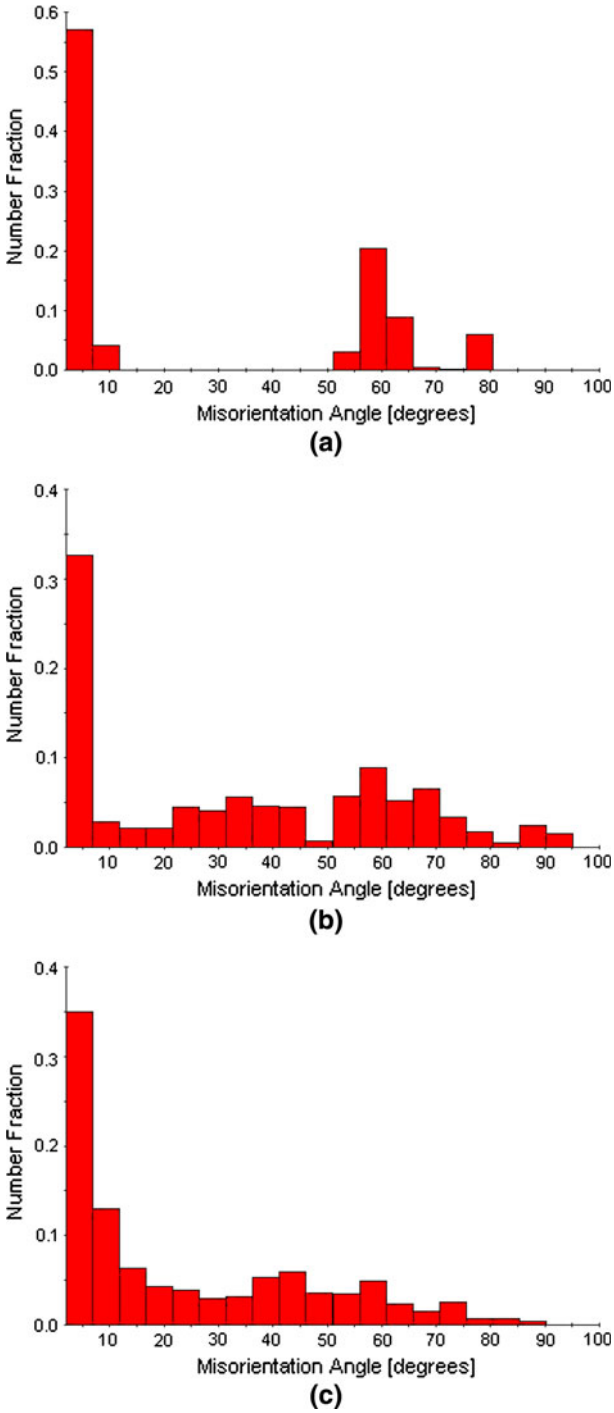

Fig. 12—Distribution of misorientation angles for four different joints after reflow using the substrate metallizations: (*a*) Cu:Cu, (*b*) Ni:Cu, and (*c*) Ni:Ni.

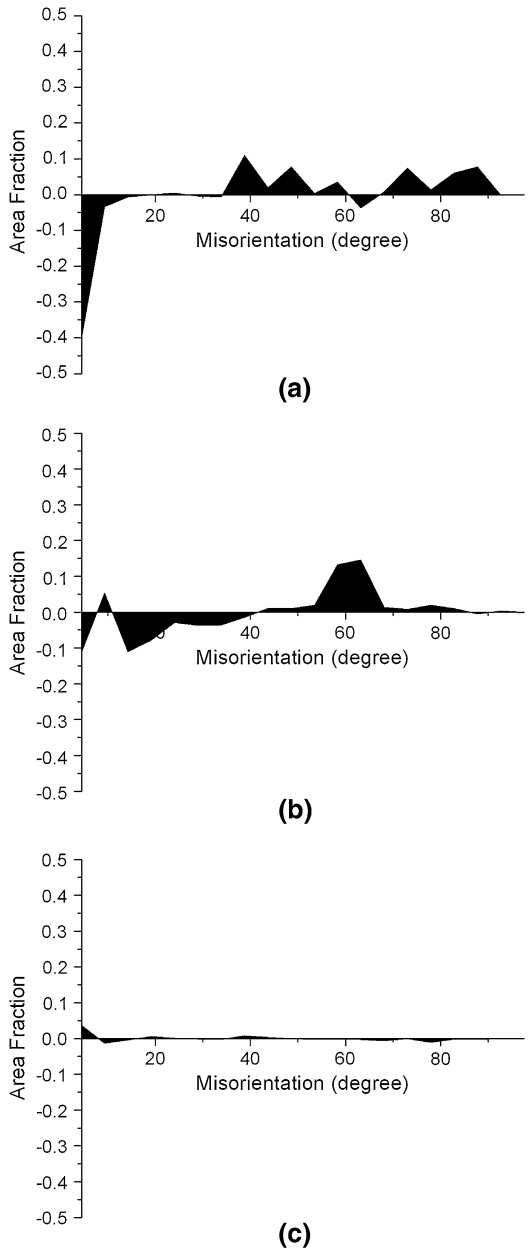

Fig. 13—Change in the distribution of misorientation angle variation after creep testing for joints with (*a*) Cu:Cu, (*b*) Ni:Cu, and (*c*) Ni:Ni metallizations.

that is dominated by grain boundary sliding ordinarily has a stress exponent of 2 or less. However, even if grain boundary mobility is not rate determining, it is ordinarily a significant contributor to deformation and, hence, to the creep rate. Put simply, each step of the rate-determining mechanism causes an increment of deformation that includes deformation due to grain boundary sliding or reconfiguration. The higher the grain boundary mobility, the greater that increment will be. Since the increment of strain per rate-controlling step is contained in the pre-exponential factor, A, it follows that A should increase with grain boundary mobility.

IV. CONCLUSIONS

The creep rate of Sn solder joints is significantly affected by the joint metallization. Cu|Sn|Cu joints have significantly higher creep rates than Ni|Sn|Cu

joints, which have higher creep rates than Ni|Sn|Ni joints. Replacing Ni by Cu on both sides increases the creep rate at 333 K (60 °C) by roughly an order of magnitude. The creep rate increased with no apparent change in the dominant creep mechanism; the change in the constitutive equation for creep (the Dorn equation) is in the pre-exponential factor. The increased creep rate on replacing Ni by Cu is accompanied by a decrease in the microhardness of polygranular samples, but an increase in the nanohardness measured in the grain interiors.

The apparent reason for the increase in polygranular hardness and creep resistance when Cu metallization is replaced by Ni is a dramatic decrease in grain boundary mobility due to the introduction of a dense array of Ni_3Sn_4 intermetallic precipitates along the grain boundaries. These inhibit grain boundary sliding, boundary reconfiguration, and grain growth during creep. The lower nanohardness of the Ni|Sn|Ni joint is due to the relatively low diffusivity of Ni, which has the consequence that the hardening precipitates are essentially confined to the boundaries. The intermediate creep rate of the asymmetric Ni|Sn|Cu joint has two causes. As in the Ni-Ni joint, grain boundary mobility is restricted by intergranular precipitates. These have a Cu_6Sn_5 structure, but apparently contain some Ni, which increases their density and biases their distribution toward the grain boundaries, where Ni is more accessible. The nominal creep rate of the Ni|Sn|Cu joint is also decreased by the morphology of the interfacial intermetallic. A thick distribution of $(Cu,Ni)_6Sn_5$ whiskers develops on the Ni side. These whiskers pin the solder so that only a part of the joint cross section actually deforms in creep.

ACKNOWLEDGMENTS

This work was supported by Intel Corporation through a gift to the University of California, Berkeley. The authors also acknowledge support, *via* access to facilities and equipment, from the National Center for Electron Microscopy, Lawrence Berkeley National Laboratory, which is supported by the United States Department of Energy under Contract No. DE-AC02-05CH11231.

OPEN ACCESS

This article is distributed under the terms of the Creative Commons Attribution Noncommercial License which permits any noncommercial use, distribution, and reproduction in any medium, provided the original author(s) and source are credited.

REFERENCES

1. H.J. Frost and M.F. Ashby: *Deformation-Mechanism Maps*, Pergamon, New York, NY, 1982.
2. Y. Kariya and M. Otsuka: *J. Electron. Mater.*, 1998, vol. 27 (11), pp. 1229–35.
3. C. Kanchanomai, Y. Miyahita, and Y. Mutoh: *Int. J. Fatigue*, 2002, vol. 24, pp. 671–83.
4. J. Liang, N. Gollhardt, P.S. Lee, S.A. Schroeder, and W.L. Morris: *Fatigue Fract. Eng. Mater. Struct.*, 1996, vol. 19 (11), pp. 1401–09.
5. C. Kanchanomai, S. Yamamoto, Y. Miyahsita, Y. Mutoh, and A.J. Mcevily: *Int. J. Fatigue*, 2002, vol. 24, pp. 57–67.
6. S. Wen, L.M. Keer, and H. Mavoori: *J. Electron. Mater.*, 2001, vol. 30 (9), pp. 1190–96.
7. J. Zhao, Y. Mutoh, Y. Miyashita, and S.L. Mannan: *J. Electron. Mater.*, 2002, vol. 31 (8), pp. 879–86.
8. H.G. Song, J.W. Morris, Jr., and F. Hua: *JOM*, 2002, vol. 54 (6), pp. 30–32.
9. D.K. Joo, S.W. Shin, K.O. Lee, and Jin Yu: *52th ECTC,* 2002, pp. 1221–25.
10. S.K. Kang, W.K. Choi, D.Y. Shin, P. Lauro, D.W. Henderson, T. Gosselin, and D.N. Leonard: *52th ECTC*, 2002, pp. 146–53.
11. S.J. Zaefferer: *Appl. Cryst.*, 2000, vol. 30, pp. 10–25.
12. J.E. Bird, A.K. Mukherjee, and J.E. Dorn: *Quantitative Relation between Properties and Microstructure*, D.G. Brandon and A. Rosen, eds., Israel University Press, Jerusalem, Israel, 1969, p. 255.
13. J.W. Morris, Jr. and H.L. Reynolds: in *Design and Reliability of Solders and Solder Interconnections*, R.K. Mahidhara, D.R. Frear, S.M.L. Sastry, K.L. Murty, P.K. Liaw, and W. Winterbottom, eds., TMS, Warrendale, PA, 1997, p. 49.
14. M. Kerr and N. Chawla: *Acta Mater.*, 2004, vol. 52, pp. 4527–35.
15. R. Lagneborg and B. Bergman: *Met. Sci.*, 1976, vol. 10, pp. 10–20.
16. K.O. Lee, J.W. Morris, Jr., and F. Hua: *10th Int. Symp. on Advanced Packaging Materials: Processes, Properties and Interfaces (IEEE Cat. No. 05TH8808)*, IEEE, Piscataway, NJ, 2005, pp. 17–20.
17. A.U. Telang, T.R. Bieler, D.E. Mason, and K.N. Subramanian: *J. Electron. Mater.*, 2003, vol. 32, pp. 1455–62.
18. N. Chawla and R.S. Sidhu: *J. Mater. Sci., Materials in Electronics, Special Issue on Pb-Free Solders*, 2007, vol. 18, pp. 175–89.
19. S.J. Wang and C.Y. Liu: *J. Electron. Mater.*, 2003, vol. 32, pp. 1303–09.
20. A.U. Telang, T.R. Bieler, S. Choi, and K.N. Subramanian: *J. Mater. Res.*, 2002, vol. 17, pp. 2294–2306.
21. S. Tosima, S. Harada, and E.O. Johnson: *RCA (Radio Corporation of America) Rev.*, 1984, vol. 45, pp. 90–108.